Long-Distance Electron Transport in Multicellular Freshwater Cable Bacteria

Tingting Yang[a#], Marko S. Chavez[a#], Christina M. Niman[a], Shuai Xu[a], Mohamed Y. El-Naggar[a,b,c,*]

[#]Authors contributed equally
[a] Department of Physics and Astronomy, University of Southern California, Los Angeles, CA 90089; [b] Molecular and Computational Biology Section, Department of Biological Sciences, University of Southern California, Los Angeles, CA 90089; [c] Department of Chemistry, University of Southern California, Los Angeles, CA 90089

*To whom correspondence should be addressed.
University of Southern California, 1002 Childs Way, MCB 220Q, Los Angeles, CA 90089-3502
(213) 740-2394; mnaggar@usc.edu

Abstract

Filamentous multicellular cable bacteria perform centimeter-scale electron transport in a process that couples oxidation of an electron donor (sulfide) in deeper sediment to the reduction of an electron acceptor (oxygen or nitrate) near the surface. While this electric metabolism is prevalent in both marine and freshwater sediments, detailed electronic measurements of the conductivity previously focused on the marine cable bacteria (*Candidatus* Electrothrix), rather than freshwater cable bacteria, which form a separate genus (*Candidatus* Electronema) and contribute essential geochemical roles in freshwater sediments. Here, we characterize the electron transport characteristics of *Ca.* Electronema cable bacteria from Southern California freshwater sediments. Current-voltage measurements of intact cable filaments bridging interdigitated electrodes confirmed their persistent conductivity under a controlled atmosphere and the variable sensitivity of this conduction to air exposure. Electrostatic and conductive atomic force microscopies mapped out the characteristics of the cell envelope's nanofiber network, implicating it as the conductive pathway in a manner consistent with previous findings in marine cable bacteria. Four-probe measurements of microelectrodes addressing intact cables demonstrated nanoampere currents up to 200 μm lengths at modest driving voltages, allowing us to quantify the nanofiber conductivity at 0.1 S/cm for freshwater cable bacteria filaments under our measurement conditions. Such a high conductivity can support the remarkable sulfide-to-oxygen electrical currents mediated by cable bacteria in sediments. These measurements expand the knowledgebase of long-distance electron transport to the freshwater niche while shedding light on underlying conductive network of cable bacteria.

Significance

Cable bacteria are multicellular filaments composed of up-to-thousands of end-to-end cells and are found worldwide in both marine and freshwater sediments. Remarkably, these cells gain energy from a long-distance electron transport process that carries electrons generated by sulfide oxidation in deeper sediment layers to drive oxygen reduction near the sediment-water interface. This electric metabolism requires an unusually high electronic conductivity, previously thought impossible in natural biological materials. However, the underlying mechanism(s) remain poorly understood, and previous characterization of the conductivity largely focused on marine cable bacteria. Here, we characterize and quantify the electronic conductivity of freshwater cable bacteria from sediments in Southern California, with emphasis on the role of the conductive periplasmic fiber network in routing electron transport along cables.

Introduction

Electron transfer reactions are fundamental to biological energy conversion. Respiratory organisms, for instance, gain energy by routing electron flow from an electron donor to a terminal electron acceptor through the network of reduction-oxidation (redox) cofactors that constitute the cellular electron transport chain (1). While the length scales of biological electron transfer events were long thought to be limited to nanometer distances and confined within individual cells, recent observations of fast long-distance extracellular and intercellular electron transport in microbial communities have upended this view (2). In fact, with the discovery of micron-scale electron transport via cytochrome nanowires from metal-reducing bacteria (3, 4), conductive bacterial biofilms (5, 6), inter-species electron

58 transfer in microbial consortia (7), and multicellular cable bacteria (8), the length scales of
59 microbial electron transport observations have jumped from the nanometer to centimeter
60 scale during the last 15 years.

61 The novel multicellular filamentous cable bacteria (CB), which belong to the
62 *Desulfobulbaceae* family of Deltaproteobacteria (8), are a particularly interesting system
63 for understanding the limits of biological electron transport given that they are the only
64 known living structures capable of macroscopic (up to centimeter-scale) electron
65 conduction. This macroscopic electron transport allows CB to gain energy from coupling
66 sulfide oxidation by cells that dwell in the deeper sulfidic zone to oxygen reduction by cells
67 near the surface sediment in both marine and freshwater sediments (8-11). The energy
68 harnessed from this process allows CB to form a dense matrix (up to hundreds of meters
69 per cm^2) that composes a majority of the biomass in sediment when blooming (12-16).
70 While the molecular pathway of the conductive network responsible for centimeter-scale
71 electron transport along the cables is not yet understood, the genomic basis and components
72 allowing CB to carry out the two spatially-separated half-reactions are just beginning to
73 come into focus. CB appear to oxidize sulfide by reversing the canonical sulfate reduction
74 pathway, and are capable of sulfur disproportionation, while oxygen reduction is
75 hypothesized to be driven by periplasmic cytochromes without energy conservation due to
76 the absence of terminal oxidases (17, 18). The electrogenic sulfur oxidation and its
77 coupling to distant redox events by CB significantly affects sulfur cycling and other
78 essential geochemical processes, including nitrogen and metal cycling in global sediments
79 (18, 19).

80 But what is the conductive pathway responsible for long-distance electron transport along
81 an entire CB filament? The answer appears to lie in the unusual cell envelope of CB, where
82 up-to-thousands of cells share a common outer membrane and parallel longitudinal ridges
83 run along the surface of the entire filament (8, 20). These ridges reflect the presence of a
84 network of long nanofibers (33 – 67 nm diameter) along the entire length of each cable in
85 the periplasmic space between the common outer membrane and the cellular inner
86 membranes (20, 21). Initial electrostatic force microscopy of these ridges showed striking
87 electrostatic contrast (8), implicating the periplasmic nanofibers as the current carrying
88 structures in marine CB filaments. More recently, the conductivity of intact air-dried
89 marine CB filament and chemically extracted sheaths containing the nanofiber network
90 was measured directly by various electronic techniques (22-24). Tens of nanoampere
91 currents could be observed along both intact cable filaments and extracted nanofiber
92 sheaths spanning hundreds of microns between microelectrodes in N_2/vacuum
93 environments, but the conductance declined rapidly upon exposure to ambient air (22).
94 Conductive atomic force microscopy (C-AFM) with stiff tips that scrape outer cell surface
95 layers revealed that the conductive path indeed correlates with the network of individual
96 periplasmic nanofibers (23). For the marine CB nanofibers, conductivities spanning the 10^{-}
97 ^{2}-10^{1} S/cm range, with the upper end reaching as high as 79 S/cm, have been estimated
98 (22); these values represent a record high for any biological structure. Furthermore,
99 temperature-dependent electronic measurements suggest a thermally activated Arrhenius-
100 type charge transport process with a low activation energy, suggesting that the CB
101 conductive properties are comparable to organic semiconductor materials (24). The
102 composition of the CB conductive nanofibers remains unknown, but recent evidence points

103 to yet-unknown core proteins rich in sulfur-ligated nickel cofactors that mediate electron
104 transport through an enigmatic physical mechanism, and that the conductivity is
105 diminished upon oxidation of the Ni/S groups (25).

106 On the basis of 16S rRNA gene sequencing, the CB clade consists of two novel candidate
107 genera: the mostly marine *Candidatus* Electrothrix and mostly freshwater *Candidatus*
108 Electronema (26). In addition, a more distant group of CB has been identified in ground
109 water environments (17, 27). However, the abovementioned electronic characterization of
110 CB conduction largely focused on marine CB, with the exception of two-probe
111 measurements as part of a recent comparative study of diverse CB that included one
112 freshwater CB enrichment culture (21). Freshwater sediments can contain CB populations
113 at densities comparable to their marine counterparts, and their activity strongly influences
114 the sediment geochemistry (11). Indeed, freshwater CB play an essential role in a cryptic
115 sulfur cycle by stimulating sulfate reduction (28), and have been harnessed to significantly
116 reduce methane emissions from rice-planted soil (29). From a materials perspective,
117 investigations of freshwater CB may also uncover conductive biomaterials suited for
118 applications in less saline environments that support higher electric fields than marine
119 environments (28, 30). Here, we report on the recovery, phylogenetic analysis, imaging,
120 and electronic characterization of *Ca.* Electronema CB from Southern California
121 freshwater sediments using atomic force and multi-probe transport techniques.

122 Materials and Methods

123 **Sediment sampling and incubation.** Surface sediment and pond water was collected from
124 two sampling sites. The first site, the Ballona Freshwater Marsh pond (33°58’15”N,

118°25’51”W), is a restored wetland that was previously filled and farmed for decades and is located 18 miles from downtown Los Angeles. The pond is seasonal (accessible ~ December to early June during the wet season). The second sampling site is Mungi Lake (34°6'6.192"N, 118°0'44.2224"W), located in the Los Angeles River Basin in the city of Arcadia, California. The sediment samples were collected from shallow water because the dissolved oxygen (DO) typically declines to zero during the summer months at depths greater than 5 meters (31). In the wintertime, less water stratification results in a higher DO concentration that can support cable bacteria growth in the lake bottom sediment. Mungi Lake samples were accessible year-round despite the lake shrinking during the dry season.

The top ~5 cm of sediment from both sites was sampled approximately every 3 months. Upon returning to the laboratory, the sediment was homogenized, sieved through a 5 mm-pore-size sieve, and carefully filled into glass jars, avoiding air bubbles in the sediment. The sediment jars were then incubated in a water bath at 15 °C, submerged in circulating, air-saturated water collected from the respective sites.

Cable bacteria filaments pickup. Filamentous bacteria were detectable after 2 weeks of incubation; occasionally, the filament density was high enough to be directly observed in sediment cracks (Figure 1). Over the incubation period, small sediment cores were taken from the sediment jars using plastic straws (8 mm diameter, 80 mm length) and transferred into small petri dishes filled with DI water. Long filaments were hand-picked under a dissection microscope using glass hooks made from capillary tubes, then washed successively at least three times in MilliQ water droplets. This extraction of cable bacteria was performed in a glove bag under an N_2 atmosphere.

147 **16S rRNA gene sequence-based phylogenetic identification.** Under a dissection
148 microscope, three long filaments from each sampling site were washed and transferred into
149 a sterile PCR-tube. Cells were lysed by freeze-thaw three times as described in a previous
150 study (13). The lysates were directly used for PCR using the primer pair 8F and
151 DSBB/1297R (32). PCR was performed according to manufacturer's instructions for the
152 Q5® Hot Start High-Fidelity 2X Master Mix (New England Biolabs, USA). After 30 s at
153 98 °C for initial denaturation, PCR was performed with 35 cycles, consisting of 10 s at
154 98 °C, 30 s at 65 °C, and 45 s at 72 °C, followed by a final step of 2 min at 72 °C. The PCR
155 amplicons were mixed and cloned using a Zero Blunt™ TOPO™ PCR Cloning Kit. Clones
156 with a correct insertion were commercially sequenced (GENEWIZ, USA) using the vector
157 primers M13F and M13R. Sequences were assembled in Sequencher 5.4, and their quality
158 was checked manually. Alignment was performed in the ARB software package (arb-6.0.6)
159 (33) using aligned sequences from SILVA database SSU 132 for reference (34), and
160 manually refined subsequently. The 16S rRNA phylogenetic trees were generated by ARB.
161 Trees that were built by the ARB neighbor joining algorithm and the maximum likelihood
162 algorithm (RaxML) with a 50% positional conservation filter, with 1000 bootstrap
163 replicates in all trees, were compared to make sure the trees had no conflicting branching.
164 Representative sequences from this study were deposited in GenBank with accession
165 numbers (OR244071 - OR244134).

166 **Transmission electron microscopy (TEM).** Bundles of filaments were washed
167 thoroughly, deposited in small droplets of MilliQ water, and the CB filament-containing
168 water droplets were then transferred and air-dried on PELCO® hexagonal Carbon-Formvar
169 coated copper grids. The filament samples were unstained. High vacuum TEM was

170 performed by using an FEI Talos™ F200C (Thermo Fisher, USA) Electron Microscope at
171 80 kV, and the images were captured by a CCD camera.

172 **Electrostatic Force Microscopy (EFM).** EFM measurements were performed using an
173 Oxford Instruments Asylum Research Cypher ES atomic force microscope (AFM).
174 Substrates were affixed and electrically connected to sample discs. The CB were extracted
175 from sediment using fine glass hooks, washed several times in DI water, and placed on the
176 prepared substrates to dry. The sample discs were wired to the grounding pin of the AFM
177 upon loading. Si probes with a Ti/Ir (5/20) coating, a nominal resonant frequency of 75
178 kHz (58-97 kHz range), a nominal spring constant of 2.8 N/m (1.4-5.8 N/m range), and a
179 tip radius of 28±10 nm were used for all EFM measurements. High resolution EFM scans
180 were performed following initial 'wide view' tapping AFM imaging to locate the CB
181 filaments. For each EFM scan, a first pass scans the conductive probe in standard tapping
182 without an applied tip bias, followed by a second 'nap' pass that retraces the first pass
183 topography at a constant height above the sample. EFM was performed at different nap
184 pass heights and tip voltage biases to arrive at optimal conditions and evaluate the voltage
185 dependence. Electrostatic forces between the tip and sample shift the resonance frequency
186 of the probe, resulting in a phase change of the cantilever, which was quantified for pixels
187 representing specific features (e.g. nanofibers). The phase differences for each image (e.g.
188 specific tip voltage bias) were averaged and their standard deviation taken.

189 **Current-Voltage (I-V) measurements on Inter-Digitated Array (IDA)**
190 **Microelectrodes.** A 3 μm gap-size Au IDA (IDA Model#012129, ALS Co., Ltd, Japan)
191 and a Pine® WaveDriver 200 Bipotentiostat/Galvanostat were used for electrical
192 measurements. The IDA consists of two individually addressable arrays of interdigitated

193 gold microelectrodes (length, 2 mm; width, 3 μm; thickness: 100 nm). Copper wires were
194 affixed to these two electrodes with silver paint (Product #: 16035, TED PELLA, Inc.) and
195 covered with an epoxy layer at the contact points. The wires were then connected to the
196 potentiostat, which swept the potential from -0.2 V to 0.2 V at a 10 μV/s sweep rate. All
197 measurements were performed in an anaerobic chamber (95% N_2 and 5% H_2) (Bactron 300,
198 Sheldon Manufacturing, Inc. Cornelius, OR). Control measurements prior to
199 measurements of CB included open circuit (without water or cable bacteria), I-V
200 measurements of an IDA on which a water droplet has been deposited (no cable bacteria),
201 and I-V measurements made after the MilliQ water droplets were dried on the IDA (no
202 cable bacteria). After these controls, CB filaments were washed and deposited in a small
203 droplet of MilliQ water on the IDA surface. The CB filament-containing water droplet was
204 then left to dry prior to the I-V measurement.

205 **Conductive Atomic Force Microscopy**. Conductive atomic force microscopy (C-AFM)
206 was performed using an Oxford Instruments Asylum Research Cypher ES AFM. CB
207 filaments were placed and dried across the insulating gaps between Au (Model#012129, 3
208 μm gap) or ITO (Model#012128, 5 μm gap) IDA microelectrodes from ALS Co., Ltd,
209 Japan. For C-AFM current-mapping, ultra-sharp conductive single crystal diamond probes
210 (AD-2.8-SS, Adama Innovations, Ltd), with < 5 nm tip radius, were used to image Mungi
211 Lake CB in contact mode under N_2 perfusion. C-AFM current mapping was performed
212 with a 0.1 Hz scan rate, 300 nN force, and a constant 5 V DC voltage bias applied between
213 the probe and IDA. The probes and imaging parameters were selected to minimize
214 disturbance to the sample while simultaneously eroding the insulating outer membrane
215 enough to electrically probe the underlying periplasmic fibers. Prior to C-AFM, high

216 resolution tapping mode imaging was performed to spatially correlate the topography of
217 the CB nanofibers to conductivity.

218 Point current-voltage (I-V) measurements were also performed to measure conduction
219 along Ballona Marsh CB between the IDA microelectrodes and C-AFM tip (Si Probe
220 ASYELEC.01-R2, Oxford Instruments, with a conductive Ti/Ir (5/20) coating and 28±10
221 nm tip radius) probing CB spots above the insulating quartz IDA gap under ambient
222 conditions. At each point, the IDA voltage was swept for 5 consecutive cycles in the -10–
223 10 V range with a 0.1 cycle/second scan rate, while the C-AFM probe was grounded and
224 held in contact with the CB surface at a 450-510 nN force. All point-IV curves shown,
225 including the insulating quartz background curve, are the average values taken from the 5
226 voltage cycles.

227 **Four-probe Device Fabrication.** Four-probe (4P) microelectrode devices were designed
228 inhouse and fabricated by the University of California San Diego Nano3 cleanroom
229 foundry service. Each device consisted of a series of parallel electrode bands. The bands
230 were 3.5 mm long, 100 μm wide, and each one was connected on alternating sides to a 1.5
231 mm by 5 mm contact pad. The electrode band separation distances were variable, including
232 multiple 20 μm and 200 μm gaps to assess different CB lengths. The fabrication process is
233 briefly outlined as follows. 100 mm diameter and 0.5 mm thick SiO_2/Si wafers (Wafer
234 model: 1583, University Wafer, Inc.) were used as substrates. Solvent cleaned wafers were
235 coated with photoresist (PR) and a laser writer was used to project repeats of the device
236 pattern onto the PR with UV light. E-beam evaporation was used to deposit a 5 nm Ti
237 adhesion layer followed by a 100 nm Au layer onto the wafers. Solvents were used to

238 remove the excess Au/Ti layer and PR, leaving just the electrode patterns. As a final step,
239 the wafers were coated in PR and each device was then diced into an 18 mm x 18 mm chip.

240 **Four-probe Electrical Measurements.** Four-probe (4P) measurements were made using
241 an Agilent 4156C Precision Semiconductor Parameter Analyzer along with a Signatone
242 1160 series probe station. Thin copper wires (Product #: 1227, Train Control Systems)
243 were electrically connected to the 4P contact pads with silver paint (Product #: 16035, TED
244 PELLA, Inc.) and alligator clips attached to tungsten probes were used to connect the 4P
245 device to the analyzer. Mungi Lake CB filaments were placed and dried across the
246 electrodes of our devices. To deal with the high degree of variability between individual
247 filaments, they were placed one at a time and I-V measurements performed after each
248 deposition until current (from a conductive filament) was observed. To make the 4P
249 measurement, a set of four electrodes on the device, with either a 20 μm or a 200 μm inner
250 probe separation distance, were each wired to a source monitor unit within the analyzer.
251 Current was swept between the outer two electrodes from -1 nA to 1 nA in step sizes of
252 100 pA. The voltage difference between the inner two electrodes (V_{inner}) was then recorded
253 at each current step. Auto range voltage sensitivity with a voltage compliance of 5 V and
254 an integration time of 1 PLC were used. A 2 second delay was used between each V_{inner}
255 measurement to eliminate capacitive current contributions. Current sweeps were performed
256 three times for the two inner probe gap sizes used. Average V_{inner} values for each current
257 step were obtained from the three sweeps along with an error bar indicating the standard
258 deviation. All 4P measurements were performed under an N_2 environment.

259 The single periplasmic fiber conductivity for the CB filaments measured at each inner
260 electrode gap size was calculated from the formula $\sigma_{fiber} = \frac{L}{A\,N\,R_{cable}}$, where L is the

known spacing between the two inner electrodes, R_{cable} is the CB filament resistance, N is the average number of periplasmic fibers per cable bacteria filament, and A is the average cross-sectional area of a single periplasmic fiber. An average N = 35 fibers per CB was determined from TEM imaging. A was calculated from $\pi\left(\frac{d}{2}\right)^2$, with the periplasmic fibers assumed to be cylinders with average diameter d = 50 nm estimated from TEM imaging. R_{cable} was obtained as the inverse slope of best fit lines for the first CB current vs V_{inner} scan. Since current in each CB is carried by multiple periplasmic fibers, the $N\,R_{cable}$ factor, which represents the resistance of a single fiber, is based on a simplistic equivalent circuit model of a series of N identical parallel fiber resistors. Open circuit 2-probe controls (for each pair of electrodes on the 4P device) were performed prior to placing CB on the devices.

Results

1. Freshwater Cable Bacteria from Southern California Sediments

1.1 Identification of cable bacteria sampling sites. We identified two freshwater sediment sampling sites for recovery and subsequent measurements of cable bacteria (CB) in the Los Angeles area. The first site, Ballona Freshwater Marsh (Figure 1A), is a shallow seasonal freshwater pond which is heavily vegetated by aquatic plants that supply sufficient organic matter to the pond bottom sediment in the wet season (December to early June), and is dried out from approximately late June to December every year. The sediment profile from the site was brown-orange-colored at the surface and dark in color with a sulfide-smell below the surface, indicating a sharp oxic to sulfidic transition in the sediment. The second sampling site is Mungi Lake (Figure 1A), which is primarily fed by washes from

283 surrounding areas in Eastern Los Angeles and therefore is precipitation dependent. Mungi
284 Lake has a much thinner and more densely packed sediment layer, compared to the Ballona
285 Freshwater sediment, as the lake was converted from a gravel pit, with almost no aquatic
286 plants and therefore no roots in the bottom surface sediment.

287 **1.2 Southern California cable bacteria morphology:** Thin silk-like filaments were
288 directly observed by eye within cracks of sediment at both sampling sites. Following
289 laboratory incubation in circulating water to enrich for CB (*Materials and Methods*), a high
290 density of CB filaments was observed (Figure 1B). When observed with optical
291 microscopy, the filament diameters varied from 0.7 µm to 3 µm, with thinner CB filaments
292 usually observed within Mungi Lake sediments. Other than the diameter, there were no
293 obvious morphological difference between the CB from the two sites. Occasionally, darker
294 cells with slightly larger diameters than neighboring cells could be observed at seemingly
295 random locations along the cable filaments (Figure 1C).

296 Transmission electron microscopy (TEM) imaging revealed that the freshwater CB display
297 the characteristic previously observed parallel longitudinal periplasmic nanofibers that run
298 along the entire CB filaments (Figure 2A). The estimated width of the fibers ranged from
299 49-57 nm, which is comparable to those of the marine cables (ca. 50 nm) (20). TEM
300 imaging of CB recovered from the sediments occasionally revealed degraded cells along
301 the filaments where only an 'empty cage' of the parallel nanofibers remained, appearing as
302 darker material reflecting a higher electron-dense composition (Figure 2B) and likely
303 corresponding to the enlarged cells in Figure 1. These empty cages were previously
304 described as 'ghost filaments' which had lost all cell membrane and cytoplasm material
305 (20). Imaging of the freshwater CB also revealed small intracellular electron-dense

306 globules, consistent with polyphosphate granules commonly observed in marine cables but
307 not in freshwater CB previously (11, 18, 35). The size of polyphosphate granules in
308 freshwater CB (70 nm – 400 nm) is comparable or slightly smaller than in marine CB (35).

309 **1.3 16S rRNA gene phylogeny of Southern California freshwater cable filaments and**
310 **their associated bacteria.** Three Ballona sediment CB filaments and three Mungi Lake
311 sediment CB filaments were analyzed for 16S rRNA gene-based phylogenetic
312 identification (Figure 3). All the Ballona sequences were within the family
313 *Desulfobulbaceae*, and the majority (24/27 total Ballona sequences) grouped together with
314 the freshwater CB sequence of *Ca.* Electronema palustris (96.7% - 97.3% similarity) (26).
315 The three representative sequences slightly differ from each other indicating coexistence
316 of different species in Ballona sediment. The few non-CB sequences all affiliated to
317 sulfate-reducing bacteria from freshwater sediments (36, 37), with one sequence closely
318 related to polycyclic aromatic hydrocarbon (PAH) degrading bacteria from a novel genus
319 *Desulfoprunum benzoelyticum* (38).

320 The majority of Mungi Lake sequences affiliated within *Deltaproteobacteria* (26/35
321 clones). Three CB clones are closely related (> 99% similarity) to uncultured sequences
322 (accession number FQ658891 and FQ658831) from a PAH-contaminated wetland
323 collecting highway road runoffs (39). These Mungi Lake CB sequences share only 96.5%
324 similarity to the *Ca.* Electronema nielsenii and are even further distantly related to the
325 sequences of Ballona CB and *Ca.* Electronema palustris. Most of the non-CB Mungi Lake
326 clones (18/26 clones) grouped together to sequences identified from an altiplanic cold lake
327 in South America (40). Also in this group was a cluster (representative sequence:
328 AJ389622, similarity 98.5%) resembling uncultured sulfate-reducers from a meromictic

329 lake in Switzerland (41). Other Mungi Lake sequences affiliated to uncultured *Geobacter*
330 clones (EF192881) from a temperate artificial lake which receives mining wastes, and a
331 polychlorinated-dioxin-dechlorinating community that can also perform oxidative
332 degradation of the dechlorinated products, enriched from a polluted river sediment
333 enrichment (42). Outside the *Deltaproteobacteria*, there were few sequences belonging to
334 uncultured *Chlorobi* group (99.15% identity). One Mungi Lake clone was identified as
335 *Ignavibacteria* (98.9% similarity to CP053446), which have been consistently found as
336 the dominant flanking community in freshwater anammox bioreactors, presumably
337 reducing nitrate to nitrite and degrading peptides, amino acids and EPS produced by
338 anammox bacteria (43). One Mungi Lake clone shares 99.2% similarity to the uncultured
339 sub group 1 of *Acidobacteria* from an Australian pasture soil (2-4 cm) (44); other Mungi
340 Lake sequences include one that loosely related to a potential *Hydrogendentes* bacterium
341 (45) and 4 clones that reside deep in the branch.

342 **2. Electronic Characterization of Southern California freshwater cable bacteria**

343 **2.1 Electrostatic Force Microscopy.** Electrostatic force microscopy (EFM) was used to
344 visualize the electric field variations on Ballona CB filaments using a dual-pass
345 measurement approach. Topographic (Figure 4A) and phase (Figure 4B) tapping mode
346 images of CB were generated during the first pass, revealing in high resolution the surface
347 ridge pattern along two consecutive CB cells. During the second pass, performed with a tip
348 voltage bias at a set height (50 nm) above the retraced CB topography, the phase image
349 (Figure 4C) captured the electric force gradient distribution as a result of the change in the
350 resonant frequency of the probe arising from the CB-tip electrostatic interaction. Consistent
351 with a previous report (8), the ridges and associated nanofibers exhibited conspicuously

352 stronger electric forces relative to inter-ridge regions (Figure 4C), hinting at the unique
353 electronic properties of the underlying nanofibers. The voltage dependence of the CB-tip
354 interaction was also investigated, revealing that the phase difference between the elevated
355 ridges and inter-ridge regions is proportional to the tip voltage squared (Figure 4D).

356 **2.2 Current-voltage measurements of freshwater cable bacteria across interdigitated**
357 **array microelectrodes.** For an initial assessment of freshwater CB conduction, current-
358 voltage (I-V) measurements were performed along Ballona CB filaments bridging
359 interdigitated array (IDA) microelectrodes in the oxygen-free environment of an anaerobic
360 chamber (95% N_2, 5% H_2). In contrast to controls (open circuit IDA and deposited drops
361 lacking CB), which showed no detectable current, multiple devices with deposited CB
362 showed linear up-to-μA currents along intact filaments in response to voltage in the -0.2-
363 0.2 V range (Figure 5).

364 In contrast to previous observations of marine CB, which exhibited a rapid and massive
365 decline in conductance upon exposure to air (22), our observations of conductance in at
366 least some freshwater CB filaments hinted at a higher degree of robustness upon oxygen
367 exposure. For example, an IDA device with 2 CB filaments showed a modest slow increase
368 in conductance during repeated I-V measurements over 3 hours in the oxygen-free
369 atmosphere (Figure 5), ultimately reaching ± 3 μA in response to ± 0.2 V. Upon removal
370 from the anaerobic chamber and exposure to air, the conductance immediately declined to
371 80% of the previous value, and slowly decayed until it ultimately stabilized at 63% of the
372 oxygen-free value over 2.7 hours. When the IDA was moved back to the anaerobic chamber
373 for further I-V measurements, the conductance again increased slowly until it stabilized
374 after 2.4 hours (Figure 5). Interestingly, this behavior was filament-dependent; in another

375 IDA that started with significantly smaller conductance under N_2 flow conditions (nA
376 current values for 0.8 V), exposure to ambient air caused immediate dramatic decline
377 within minutes (Figure S1).

378 **2.3 Conductive atomic force microscopy: point current-voltage spectra.** The
379 abovementioned conductance measurements probe transport longitudinally along multiple
380 CB sections bridging IDA microelectrodes. We also performed point I-V conductance
381 measurements through CB filaments between the underlying IDA and conductive AFM
382 (C-AFM) tips; these measurements simultaneously probe longitudinal transport locally
383 along specific CB sections and transversely across specific cells to the C-AFM tip above
384 the filaments (Figure 6).

385 Tapping mode AFM images were first taken without voltage bias to visualize CB filaments
386 laid on top of IDA microelectrodes and bridging 3-5 μm sections of the insulating quartz
387 substrates (Figure 6A-C). No current response between the IDA and C-AFM tip was
388 detected in response to applied voltage when the tip then probed the bare quartz surface
389 near CBs. However, when the C-AFM tip probed points on the top surface of CB over
390 quartz gaps, we detected currents up to tens of pA for voltages (-10-10 V) between the IDA
391 and tip. These currents reflect a continuous path for electron transport from the underlying
392 IDAs into cells, longitudinally along the conductive network of CB, and transversely into
393 the overlying C-AFM tip. Interestingly, when such point I-V measurements were
394 performed on CB exposed to air, the observed conductivity did not decay immediately, but
395 slowly decreased over several hours, consistent with the IDA measurements reported above.

396 **2.4 Conductive atomic force microscopy: mapping the conductive network of cable**
397 **bacteria.** In addition to the point I-V measurements described above, C-AFM was used in

398 contact scanning mode to image the electron transport path along CB hanging off
399 microelectrodes under N_2 perfusion conditions (Figure 7). A constant voltage (5 V) was
400 applied along the freshwater CB filaments between the microelectrode and an ultra-sharp
401 (< 5 nm tip radius) conductive single crystal diamond C-AFM tip. Following a previous
402 report on marine CB (23), a force set point was selected to gently scrape off the insulating
403 outer membrane of the freshwater CB while allowing access to image the conductive
404 network underneath. Figure 7 displays a current map, stitched together from 3 consecutive
405 C-AFM images, of two CB filaments lying side-by-side and extending approximately 30
406 μm off a microelectrode. The imaging revealed parallel conductive paths consistent with
407 the periplasmic nanofibers as the charge carriers in CB. Indeed, when compared with
408 topographic imaging (Figure 7), the conductive paths coincided with the CB cell surface
409 ridge pattern.

410 **2.5 Four-probe transport measurements.** To quantify the intrinsic conductivity of
411 freshwater CB and their periplasmic nanofibers, we measured electronic transport along
412 Mungi Lake CB deposited on custom fabricated four-probe (4P) microelectrode devices.
413 In contrast to the two-probe IDA and C-AFM measurements described above, which
414 include contributions from the CB-electrode contact resistances, the 4P measurements
415 excluded contact resistance by routing current between two external microelectrodes and
416 separately measuring the voltage drop across two inner microelectrodes. Thus, our
417 quantitative estimate of CB nanofiber conductivity was made only using 4P measurements,
418 rather than conductive AFM. The resulting 4P I-V plots (Figure 8) are shown for two
419 separate inner probe separations, with the inverse slopes yielding whole CB resistances of
420 47 MΩ and 240 MΩ for the 20 μm and 200 μm lengths, respectively. By modeling the CB

421 periplasmic nanofibers as current-carrying simple cylindrical wires forming a simplified
422 circuit of parallel resistors, and taking into account each nanofiber's estimated diameter
423 (50 nm) and number of fibers per CB (~35), we arrive at a single nanofiber conductivity
424 on the order of 0.1 S/cm, from both gap sizes.

425 **Discussion**

426 The appearance in many gene sequencing studies and increasing field observations suggest
427 a cosmopolitan global distribution for cable bacteria (CB) in both marine and freshwater
428 sediments (11, 46). Here, we identified two sampling sites (Figure 1) in the Los Angeles
429 basin area, which served as a source for downstream phylogeny, microscopy, scanning
430 probe, and electronic studies of freshwater CB. While CB have not been isolated into pure
431 culture (47), the freshwater CB from both Ballona wetlands sediment and Mungi Lake
432 sediment could be reliably enriched in laboratory incubations to provide a continuous
433 supply for studies (Figure 1). Based on 16S rRNA gene sequence phylogeny (Figure 3),
434 CB from the heavily vegetated Ballona sediments are closely related to *Ca.* Electronema
435 palustris (26), which has been previously observed to associate with the roots of aquatic
436 plants (48). On the other hand, CB from the non-vegetated Mungi Lake sediments are more
437 closely related to those from PAH-contaminated sediment collecting water runoffs (39).
438 The 16S rRNA gene analysis also revealed additional non-CB clones from both Ballona
439 and Mungi Lake samples, many of which are highly similar to those from stratified and
440 oligotrophic freshwater ecosystems (34). Although the relationship and functions of these
441 bacteria are unclear, they likely represent cells firmly attached to CB filaments, as all the
442 filaments were thoroughly washed before DNA extraction. The communities from both
443 sites have representative lineages related to organic contaminant degradation, which

444 corelate to the environmental background of the two sites. In Mungi Lake, for example,
445 various contaminants (chlordane, DDT, lead, dieldrin, polycyclic aromatic hydrocarbon,
446 and polychlorinated biphenyls) have been identified previously (31).

447 Morphologically, our freshwater CB filaments exhibited the expected characteristics of
448 previously studied CB (8, 20), including the cell surface ridge pattern and underlying
449 periplasmic nanofiber network (Figures 2-4). The latter could be observed in transmission
450 electron microscopy (TEM) of freshwater CB both within intact cells and, occasionally, as
451 the remaining cage scaffold from naturally degraded cells (Figure 2). The typical single
452 nanofiber width encountered in our freshwater CB was 53 ± 8 nm, which is consistent with
453 the previously reported nanofiber thickness from marine CB (20) and recent
454 characterization of a single strain freshwater CB enrichment culture (33 nm) (21). These
455 results suggest that, while general morphological features are shared amongst diverse CB
456 strains, the number and size of the ridges (and possibly their internal components) may
457 depend on strain and environmental condition. However, similarly to previous
458 measurements of marine CB (8), electrostatic force microscopy (EFM) captured stronger
459 electric forces when scanning the cell surface above the ridges (Figure 4), again indicating
460 the unique electric potential and charge distribution from the underlying conductive
461 periplasmic nanofibers. Since EFM can also be sensitive to tip-sample distance, we report
462 the EFM phase response from a second pass performed at a fixed retrace height above the
463 sample, after acquiring the topography during the first pass. To further assess that this EFM
464 procedure is due primarily to the tip-sample electrical interaction, rather than topographic
465 crosstalk, we examined the impact of tip voltage on the EFM phase contrast (Figure 4D).
466 Since electrostatic forces are proportional to the square of the voltage at a fixed height (49),

467 the confirmation of this expected dependence unambiguously assigns EFM phase contrast
468 to the electrical properties of the sample, rather than a topographic contribution. While the
469 EFM observations qualitatively point to the unique electrical properties of CB filaments
470 and nanofibers, direct transport measurements were needed to further interrogate (Figures
471 5-7) and quantify (Figure 8) the conductivity. For example, conductive atomic force
472 microscopy (C-AFM) with an ultra-sharp diamond tip that disrupts the insulating outer cell
473 layer (Figure 7) offered a more direct confirmation of the conductivity of underlying
474 periplasmic nanofibers, by observing conductive paths between the microelectrode and
475 scanning tip that correlate with the CB ridge pattern. Furthermore, C-AFM point I-V
476 spectra (Figure 6) confirmed a direct path for charge transport originating from the
477 microelectrode below intact CB, along the internal periplasmic nanofiber, and into the C-
478 AFM tip above the sample, consistent with the previously observed interconnectivity of
479 the nanofiber network between cells (23). The latter measurements also illustrate a high
480 degree of variability (Figure 6) in the conduction signal across different cables; it remains
481 unclear whether this variability reflects heterogeneities intrinsic to different CB filaments
482 or stems from culturing and/or sample preparation effects (including possible oxidative
483 damage). Taken collectively, however, the EFM and C-AFM observations, performed here
484 for the first time on freshwater CB, are consistent with previous analogous measurements
485 on marine CB (8, 22, 23).

486 While their two-probe nature includes a contact resistance contribution, we found
487 interdigitated array (IDA) microelectrodes to offer a convenient assessment of CB
488 conduction properties (Figure 5) ahead of more sophisticated AFM and four-probe based
489 techniques (Figures 6-8). The IDA platforms, which are commercially available, have been

490 previously used to investigate conductivity in bacterial biofilms (5, 6), and result in high
491 current signals (μA currents in Figure 5) as a result of assessing transport along multiple
492 CB sections spanning the IDA inter-electrode gaps. Interestingly, these measurements hint
493 that freshwater CB conductivity may have a somewhat higher degree of tolerance to
494 oxygen exposure than previously reported for marine CB. Instead of an instantaneous and
495 dramatic decline in conduction upon exposure to air (22), some of our freshwater CB
496 samples exhibited a slow (hours) and only partial decline of the conduction upon exposure
497 to air, which could be partially restored by re-insertion into an anaerobic chamber (Figure
498 5). While these observations showed a high degree of variability and therefore require a
499 more detailed investigation, it is interesting to consider the possibility that the oxidative
500 decline (or other damaging processes), thought to be a consequence of oxidation of Ni
501 cofactors involved in electron transport (25), may not affect all sections of the cm long CB
502 filaments simultaneously; under these conditions, IDA measurements, which probe
503 multiple micrometer-scale electrode-crossing CB regions (e.g. 372 crossings in Figure 5
504 inset) may offer an advantage over techniques addressing entire CBs or specific CB regions.
505 It is also interesting to consider an alternative possibility that the conductive properties of
506 freshwater CB maybe intrinsically more oxygen-resistant than marine CB. For example, a
507 recent comparative study (21) hints at significant differences in the morphology, number,
508 and size of nanofibers when comparing a marine CB strain to a freshwater CB strain.
509 Specifically, while the marine CB was characterized by a 50% larger cross-sectional area
510 per nanofiber, the total nanofibers' area was 40% smaller than the freshwater strain due to
511 a smaller number of nanofibers per CB filament. Given the proposed central role of
512 nanofibers in mediating electron transport along CB, it is possible that such differences

513 may also lead to different degrees of tolerance against oxidative degradation upon exposure
514 to air. In general, salt content affects the solubility of oxygen, which dissolves to 25% high
515 levels in fresh water than saltwater. Indeed, previous CB studies verified 20% - 25% higher
516 oxygen concentration at the surface of freshwater sediment (310 – 350 μM) (11, 28),
517 compared to marine sediments (200 – 280 μM) (8-10, 13, 14, 35, 50-52). Our results
518 motivate a systematic investigation to correlate the oxygen availability in CB environments
519 to both their conductivity and tolerance of electron transport to oxygen exposures.

520 When taking contact resistances of intact freshwater CB into account with four-probe
521 measurements (Figure 8), we estimated the single nanofiber conductivity to be in the 10^{-1}
522 S/cm range. Since CB may possess nonuniform conductivity along their length and since
523 estimates for nanofiber diameter and per cable density were used in our single nanofiber
524 conductivity calculation, we cannot constrain our reported value to better than order 10^{-1}
525 S/cm. However, our figure falls within the 10^{-2}-10^{1} S/cm range recently reported for marine
526 CB (22, 24). We did not observe freshwater CB nanofiber conductivity near the upper end
527 of the previously reported range (~80 S/cm) (22). While these measurements are performed
528 under *ex situ* conditions, they motivate the question of whether the measured conductivities
529 are sufficient to support the *in situ* activity of CB in sediments. From previous
530 measurements of the CB filaments density in sediment incubations (~10^{8} - 10^{9} m^{-2}) and the
531 electron current densities linking electrogenic sulfur oxidation to oxygen reduction (74 -
532 96 mA m^{-2}) (10, 13, 53, 54), one arrives at a per cable current around 170 pA, which
533 amounts to per nanofiber current of 5 pA given the average number of nanofibers seen in
534 our cables. Assuming a driving voltage up to 1 V, representing the redox potential
535 difference between the anodic sulfide oxidation and cathodic oxygen reduction half-

536 reactions, for a typical nanofiber cross sectional area and length (e.g. several mm), these
537 conditions require a minimum nanofiber conductivity on the order of 0.1 S/cm.
538 Remarkably, this heuristic calculation therefore sets a limit on conductivity that is
539 consistent with the electronic measurements. It is also interesting to consider what the
540 observed conductivities (22-24) and this study may teach us about the underlying physical
541 electron transport mechanism in CB. It is common to interpret such extended transport in
542 molecular systems in one of two limits: hopping between charge localizing sites such as
543 redox factors (e.g. the hypothesized Ni/S groups of CB), or coherent band-like transport
544 familiar from periodic systems including metals or semiconductors. In this context, the
545 thermally activated nature of CB transport, and the estimate of the room temperature
546 electron mobility at ~ 0.1 cm^2/Vs (24) are consistent with hopping transport, as the latter
547 figure approaches but is still below the generally accepted minimum mobility (~1 cm^2/Vs)
548 for band transport (55, 56). Still, future electronic transport and structural studies (e.g. to
549 identify the precise molecular makeup of the nanofibers) are needed to resolve the
550 underlying mechanism, particularly if conduction operates in a more complex regime than
551 band theory or hopping, where electron transport may be delocalized transiently or
552 permanently over several sites along the nanofibers (57, 58).

553 **Conclusion**

554 In summary, this study presents a detailed electronic characterization of *Candidatus*
555 Electronema cable bacteria from Southern California freshwater sediments. The cell
556 envelope characteristics of the freshwater cable bacteria, including the characteristic
557 periplasmic nanofiber network, are consistent with previous observations of the globally
558 distributed cable bacteria. Conductive atomic force and electrostatic force microscopies

confirmed the role of the nanofiber network as the conductive conduit of freshwater cable bacteria, as previously observed in marine cable bacteria. In addition, current-voltage measurements confirmed the conductivity of whole cable bacterial filaments, while hinting that the conductivity of the freshwater filaments may be less sensitive to oxygen exposure than previously observed. The conductivity of the periplasmic nanofibers from four-probe electronic transport measurements was estimated at 0.1 S/cm, a value high enough to support the electron current densities linking sulfide oxidation to oxygen reduction through the electric metabolism of cable bacteria in sediment environments. While electronic characterization of this long-distance electron transport previously focused on marine cables, our measurements shed light on the conductivity of freshwater cable bacteria, and highlight the potential applications of cable bacteria as bioelectronic conduits with both environmental and future biotechnological relevance.

Acknowledgments

This work was supported by supported by the W.M. Keck Foundation award 8626 and Gordon and Betty Moore Foundation grant 10148. We thank Dr. Edith Read and the Friends of Ballona Wetlands organization for their kind help and sampling permission. We would like to thank the Nano3 cleanroom at the University of California, San Diego for microfabrication services. TEM imaging was performed at the Core Center of Excellence in Nano Imaging at the University of Southern California.

References

1. Gray HB & Winkler JR (2003) Electron tunneling through proteins. *Q Rev Biophys* 36(3):341-372.
2. Atkinson JT, Chavez MS, Niman CM, & El-Naggar MY (2023) Living electronics: A catalogue of engineered living electronic components. *Microbial Biotechnology* 16(3):507-533.
3. Wang FB*, et al.* (2019) Structure of Microbial Nanowires Reveals Stacked Hemes that Transport Electrons over Micrometers. *Cell* 177(2):361-+.
4. Wang FB*, et al.* (2022) Structure of Geobacter OmcZ filaments suggests extracellular cytochrome polymers evolved independently multiple times. *Elife* 11.
5. Yates MD*, et al.* (2016) Measuring conductivity of living Geobacter sulfurreducens biofilms. *Nat Nanotechnol* 11(11):910-913.
6. Xu S, Barrozo A, Tender LM, Krylov AI, & El-Naggar MY (2018) Multiheme Cytochrome Mediated Redox Conduction through Shewanella oneidensis MR-1 Cells. *J Am Chem Soc* 140(32):10085-10089.
7. McGlynn SE, Chadwick GL, Kempes CP, & Orphan VJ (2015) Single cell activity reveals direct electron transfer in methanotrophic consortia. *Nature* 526(7574):531-535.
8. Pfeffer C*, et al.* (2012) Filamentous bacteria transport electrons over centimetre distances. *Nature* 491(7423):218-221.
9. Nielsen LP, Risgaard-Petersen N, Fossing H, Christensen PB, & Sayama M (2010) Electric currents couple spatially separated biogeochemical processes in marine sediment. *Nature* 463(7284):1071-1074.
10. Meysman FJR, Risgaard-Petersen N, Malkin SY, & Nielsen LP (2015) The geochemical fingerprint of microbial long-distance electron transport in the seafloor. *Geochim Cosmochim Ac* 152:122-142.
11. Risgaard-Petersen N*, et al.* (2015) Cable Bacteria in Freshwater Sediments. *Appl Environ Microbiol* 81(17):6003-6011.
12. Marzocchi U*, et al.* (2018) Transient bottom water oxygenation creates a niche for cable bacteria in long-term anoxic sediments of the Eastern Gotland Basin. *Environmental microbiology* 20(8):3031-3041.
13. Schauer R*, et al.* (2014) Succession of cable bacteria and electric currents in marine sediment. *ISME J* 8(6):1314-1322.
14. Malkin SY*, et al.* (2014) Natural occurrence of microbial sulphur oxidation by long-range electron transport in the seafloor. *ISME J* 8(9):1843-1854.
15. Burdorf LDW, Hidalgo-Martinez S, Cook PLM, & Meysman FJR (2016) Long-distance electron transport by cable bacteria in mangrove sediments. *Mar Ecol Prog Ser* 545:1-8.
16. van de Velde S*, et al.* (2016) The impact of electrogenic sulfur oxidation on the biogeochemistry of coastal sediments: A field study. *Geochim Cosmochim Ac* 194:211-232.
17. Muller H, Marozava S, Probst AJ, & Meckenstock RU (2020) Groundwater cable bacteria conserve energy by sulfur disproportionation. *ISME J* 14(2):623-634.
18. Kjeldsen KU*, et al.* (2019) On the evolution and physiology of cable bacteria. *Proc Natl Acad Sci U S A* 116(38):19116-19125.
19. Marzocchi U*, et al.* (2014) Electric coupling between distant nitrate reduction and sulfide oxidation in marine sediment. *ISME J* 8(8):1682-1690.
20. Cornelissen R*, et al.* (2018) The Cell Envelope Structure of Cable Bacteria. *Frontiers in microbiology* 9.
21. Digel L*, et al.* (2023) Comparative electric and ultrastructural studies of cable bacteria reveal new components of conduction machinery. *bioRxiv*:2023.2005.2024.541955.

22. Meysman FJR, *et al.* (2019) A highly conductive fibre network enables centimetre-scale electron transport in multicellular cable bacteria. *Nature communications* 10(1):4120.
23. Thiruvallur Eachambadi R, *et al.* (2020) An Ordered and Fail-Safe Electrical Network in Cable Bacteria. *Advanced biosystems* 4(7):e2000006.
24. Bonne R, *et al.* (2020) Intrinsic electrical properties of cable bacteria reveal an Arrhenius temperature dependence. *Sci Rep-Uk* 10(1).
25. Boschker HTS, *et al.* (2021) Efficient long-range conduction in cable bacteria through nickel protein wires. *Nature communications* 12(1).
26. Trojan D, *et al.* (2016) A taxonomic framework for cable bacteria and proposal of the candidate genera Electrothrix and Electronema. *Systematic and applied microbiology* 39(5):297-306.
27. Muller H, *et al.* (2016) Long-distance electron transfer by cable bacteria in aquifer sediments. *ISME J* 10(8):2010-2019.
28. Sandfeld T, Marzocchi U, Petro C, Schramm A, & Risgaard-Petersen N (2020) Electrogenic sulfide oxidation mediated by cable bacteria stimulates sulfate reduction in freshwater sediments. *ISME J* 14(5):1233-1246.
29. Scholz VV, Meckenstock RU, Nielsen LP, & Risgaard-Petersen N (2020) Cable bacteria reduce methane emissions from rice-vegetated soils. *Nature communications* 11(1):1878.
30. Risgaard-Petersen N, Damgaard LR, Revil A, & Nielsen LP (2014) Mapping electron sources and sinks in a marine biogeobattery. *Journal of Geophysical Research-Biogeosciences* 119(8):1475-1486.
31. Environmental-Protection-Agency US (2012) Los Angeles Area Lakes Total Maximum Daily Loads-- Section 4 Peck Road Park Lake https://19january2017snapshot.epa.gov/www2013/region2019/water/tmdl/la-lakes/LALakesTMDLsSection2014PeckRoadParkLake.pdf.
32. Kjeldsen KU, *et al.* (2007) Diversity of sulfate-reducing bacteria from an extreme hypersaline sediment, Great Salt Lake (Utah). *FEMS microbiology ecology* 60(2):287-298.
33. Ludwig W, *et al.* (2004) ARB: a software environment for sequence data. *Nucleic Acids Res* 32(4):1363-1371.
34. Quast C, *et al.* (2013) The SILVA ribosomal RNA gene database project: improved data processing and web-based tools. *Nucleic Acids Res* 41(D1):D590-D596.
35. Sulu-Gambari F, *et al.* (2016) Cable Bacteria Control Iron-Phosphorus Dynamics in Sediments of a Coastal Hypoxic Basin. *Environ Sci Technol* 50(3):1227-1233.
36. Sass H, Wieringa E, Cypionka H, Babenzien HD, & Overmann J (1998) High genetic and physiological diversity of sulfate-reducing bacteria isolated from an oligotrophic lake sediment. *Arch Microbiol* 170(4):243-251.
37. Ferrer M, *et al.* (2011) Taxonomic and Functional Metagenomic Profiling of the Microbial Community in the Anoxic Sediment of a Sub-saline Shallow Lake (Laguna de Carrizo, Central Spain). *Microbial Ecology* 62(4):824-837.
38. Junghare M & Schink B (2015) Desulfoprunum benzoelyticum gen. nov., sp. nov., a Gram-stain-negative, benzoate-degrading, sulfate-reducing bacterium isolated from a wastewater treatment plant. *International journal of systematic and evolutionary microbiology* 65(Pt 1):77-84.
39. Martin F, *et al.* (2012) Betaproteobacteria dominance and diversity shifts in the bacterial community of a PAH-contaminated soil exposed to phenanthrene. *Environmental pollution* 162:345-353.
40. Dorador C, Vila I, Witzel KP, & Imhoff JF (2013) Bacterial and archaeal diversity in high altitude wetlands of the Chilean Altiplano. *Fund Appl Limnol* 182(2):135-159.

41. Tonolla M, Demarta A, Peduzzi S, Hahn D, & Peduzzi R (2000) In situ analysis of sulfate-reducing bacteria related to Desulfocapsa thiozymogenes in the chemocline of meromictic Lake Cadagno (Switzerland). *Appl Environ Microb* 66(2):820-824.
42. Dorador C, Castillo G, Witzel KP, & Vila I (2007) Bacterial diversity in the sediments of a temperate artificial lake, Rapel reservoir. *Rev Chil Hist Nat* 80(2):213-224.
43. Ali M, Shaw DR, Albertsen M, & Saikaly PE (2020) Comparative Genome-Centric Analysis of Freshwater and Marine ANAMMOX Cultures Suggests Functional Redundancy in Nitrogen Removal Processes. *Frontiers in microbiology* 11.
44. Sait M, Hugenholtz P, & Janssen PH (2002) Cultivation of globally distributed soil bacteria from phylogenetic lineages previously only detected in cultivation-independent surveys. *Environmental microbiology* 4(11):654-666.
45. Momper L, Aronson HS, & Amend JP (2018) Genomic Description of 'Candidatus Abyssubacteria,' a Novel Subsurface Lineage Within the Candidate Phylum Hydrogenedentes. *Frontiers in microbiology* 9.
46. Burdorf LDW*, et al.* (2017) Long-distance electron transport occurs globally in marine sediments. *Biogeosciences* 14(3):683-701.
47. Thorup C*, et al.* (2021) How to grow your cable bacteria: Establishment of a stable single-strain culture in sediment and proposal of Candidatus Electronema aureum GS. *Systematic and applied microbiology* 44(5).
48. Scholz VV*, et al.* (2021) Cable bacteria at oxygen-releasing roots of aquatic plants: a widespread and diverse plant-microbe association. *New Phytologist* 232(5):2138-2151.
49. Staii C, Johnson AT, & Pinto NJ (2004) Quantitative analysis of scanning conductance microscopy. *Nano Letters* 4(5):859-862.
50. Risgaard-Petersen N, Revil A, Meister P, & Nielsen LP (2012) Sulfur, iron-, and calcium cycling associated with natural electric currents running through marine sediment. *Geochim Cosmochim Ac* 92:1-13.
51. Larsen S, Nielsen LP, & Schramm A (2015) Cable bacteria associated with long-distance electron transport in New England salt marsh sediment. *Environ Microbiol Rep* 7(2):175-179.
52. Seitaj D*, et al.* (2015) Cable bacteria generate a firewall against euxinia in seasonally hypoxic basins. *P Natl Acad Sci USA* 112(43):13278-13283.
53. Geelhoed JS, van de Velde SJ, & Meysman FJR (2020) Quantification of Cable Bacteria in Marine Sediments via qPCR. *Frontiers in microbiology* 11.
54. van de Velde S, Callebaut I, Gao Y, & Meysman FJR (2017) Impact of electrogenic sulfur oxidation on trace metal cycling in a coastal sediment. *Chemical Geology* 452:9-23.
55. Polizzi NF, Skourtis SS, & Beratan DN (2012) Physical constraints on charge transport through bacterial nanowires. *Faraday Discuss* 155:43-62.
56. Pirbadian S & El-Naggar MY (2012) Multistep hopping and extracellular charge transfer in microbial redox chains. *Phys Chem Chem Phys* 14:13802-13808.
57. Beratan DN (2019) Why Are DNA and Protein Electron Transfer So Different? *Annu Rev Phys Chem* 70:71-97.
58. Beratan DN*, et al.* (2015) Charge Transfer in Dynamical Biosystems, or The Treachery of (Static) Images. *Accounts Chem Res* 48(2):474-481.

Figures and Tables

Figure 1. (A) Sampling sites for cable bacteria from the Ballona Freshwater Marsh and Mungi Lake, California, USA. **(B)** Enrichment in laboratory incubations resulted in a high density of long cable bacteria filaments, some of which could be observed directly in cracked sediments. Scale bar: 35 mm. **(C)** Optical microscopy revealed the characteristic end-to-end multicellular morphology of the cable bacteria filaments, revealing occasional darker cells (black arrows) with slightly larger diameters, consistent with 'empty cage' cells scaffolded by the nanofiber network of cable bacteria (see Figure 2). Scale bar: 5 µm.

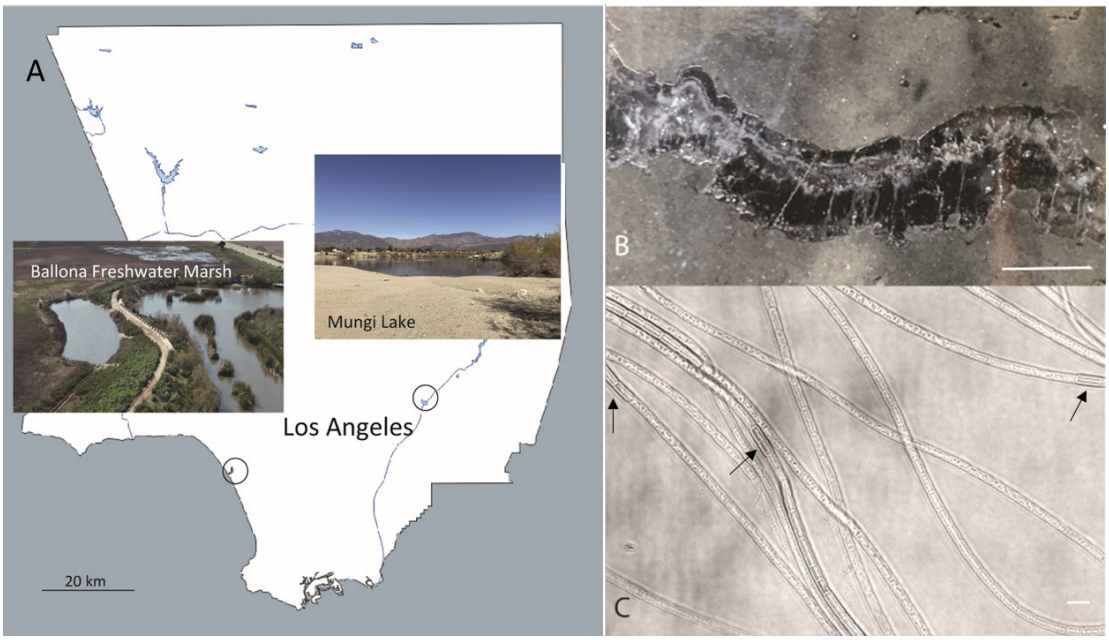

Figure 2. (A) Transmission electron microscopy of Ballona Freshwater Marsh cable bacteria showing the characteristic cell surface ridge pattern. Scale bar: 1 µm. (B) The underlying network of parallel periplasmic nanofibers can be seen clearly in occasional degraded cells as the electron-dense scaffold of "empty cages". Small intracellular dark globules (white arrows) are consistent with polyphosphate granules commonly found in marine cable filaments. Scale bar: 2.5 µm.

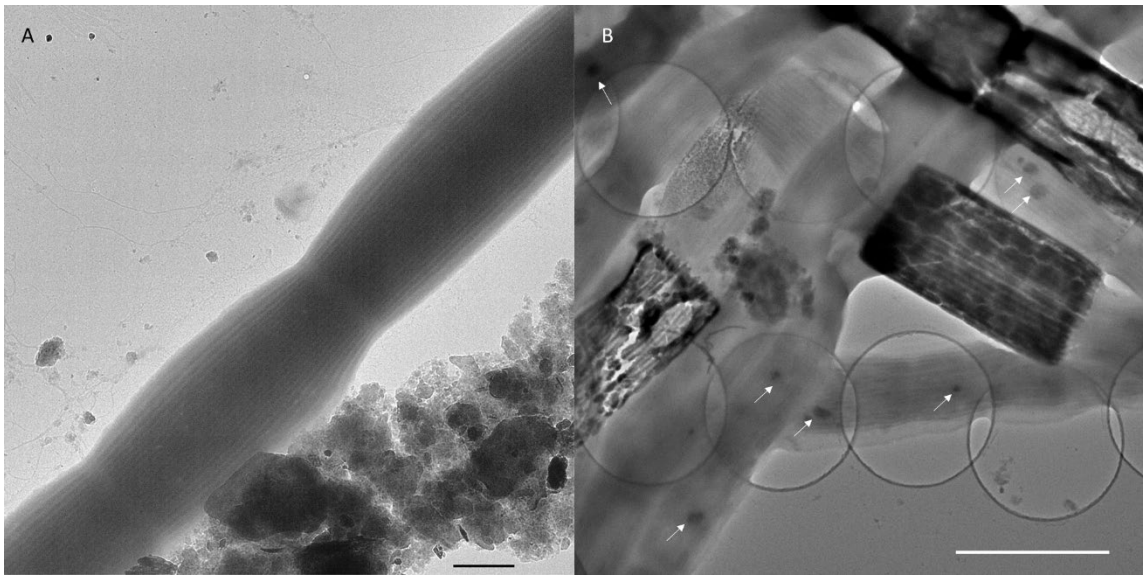

735 **Figure 3.** Phylogenetic tree based on 16S rRNA gene sequences of the Ballona Freshwater
736 Marsh and Mungi Lake cable bacteria, other cable bacterial Candidatus taxa, and
737 representatives of isolated members from the family *Desulfobulbaceae*. Scale bar
738 represents 10% estimated sequence divergence. Bootstrap numbers (1000 re-samplings) >
739 70 are listed.

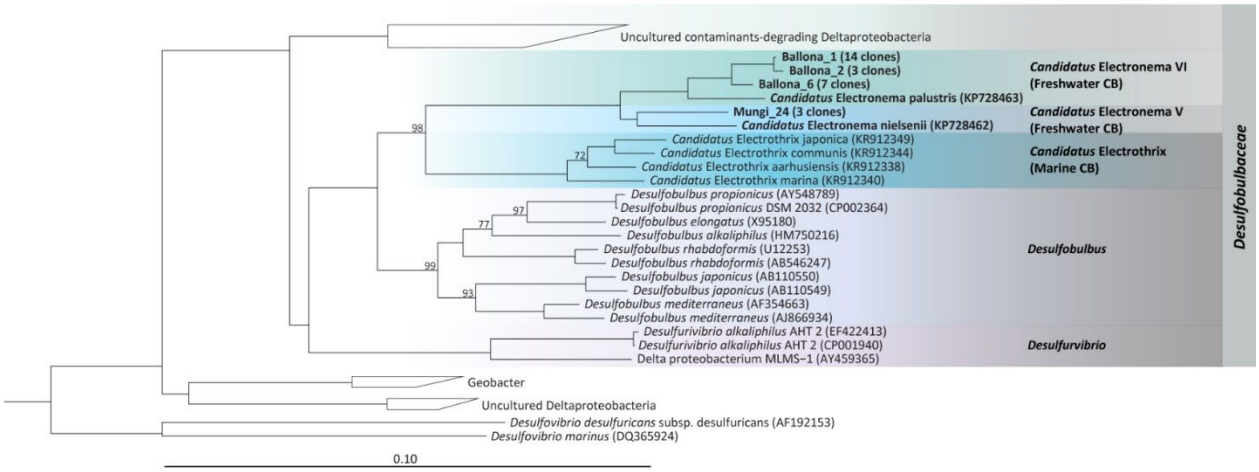

Figure 4. (A) Tapping mode atomic force microscopy of freshwater cable bacteria near the junction between two cells. Inset is a cross-sectional line scan showing cell surface ridge pattern. **(B)** Atomic force phase image corresponding to the topographical scan and showing the ridge pattern in high contrast. **(C)** Electrostatic force microscopy image with a 6 V tip bias, collected from the retrace scan at 50 nm fixed height above the cable surface. The contrast in this image stems from the electric force rather than topography. **(D)** The voltage dependence of the electrostatic interaction (phase shift, $\Delta\phi$, of the ridges with higher electric force relative to inter-ridge regions) between the conductive tip and the same cable bacterial filament from (C).

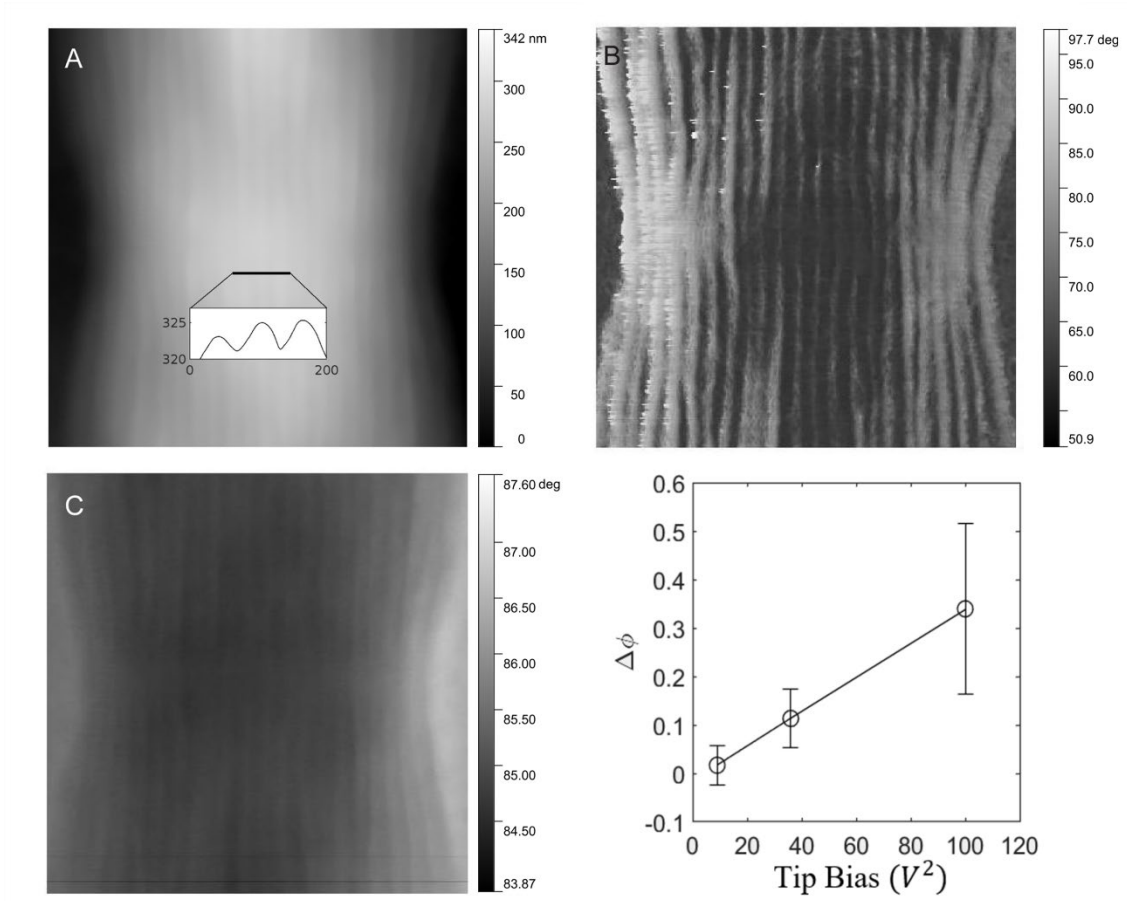

Figure 5. Current-voltage (I-V) measurements of Ballona Freshwater Marsh cable bacteria on gold interdigitated array (IDA) microelectrodes (3 µm gap between the fingers of the two electrode bands). For this measurement, two cable filaments were deposited on the IDA (inset upper-left). The I-V measurements (black) show a modest increase in conductance over time (3 hours) during consecutive measurements in an air-free environment (95% N_2 and 5% H_2). Upon air exposure (red) the conductance slowly declined over time (2.7 hours), and conductance recovered partially after re-insertion into an air-free environment (green). Arrow direction denotes measurements over time for a particular condition. The lower right inset demonstrates the resistivity change over time at different conditions.

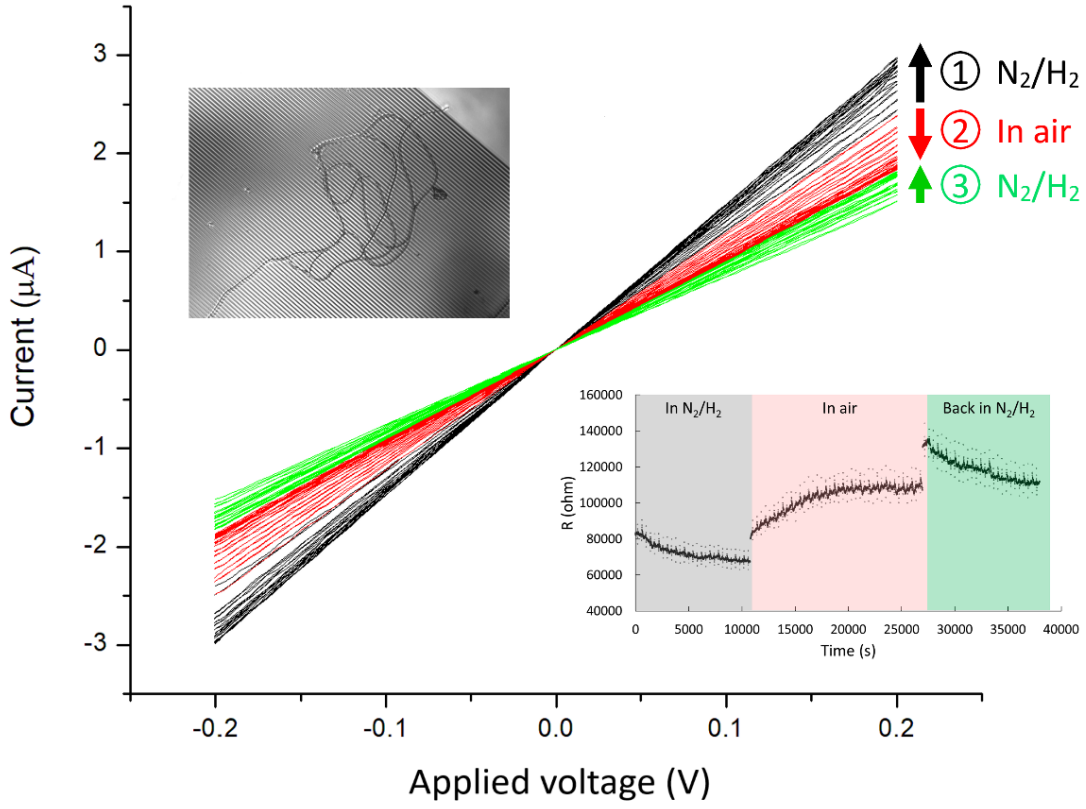

Figure 6. Representative atomic force microscopy amplitude images of Ballona freshwater cable bacteria filaments spanning the insulating quartz gap between yellow false colored gold **(A and B)** and indium tin oxide **(C)** microelectrodes. Colored crosses mark the conductive tip location in each sample where point current-voltage (I-V) spectra were collected to measure electron transport between the microelectrodes and tip. Scale bars: 2.5 µm. **(D)** I-V responses from the three representative cables. Line color corresponds to the color of the corresponding cross mark in (A-C).

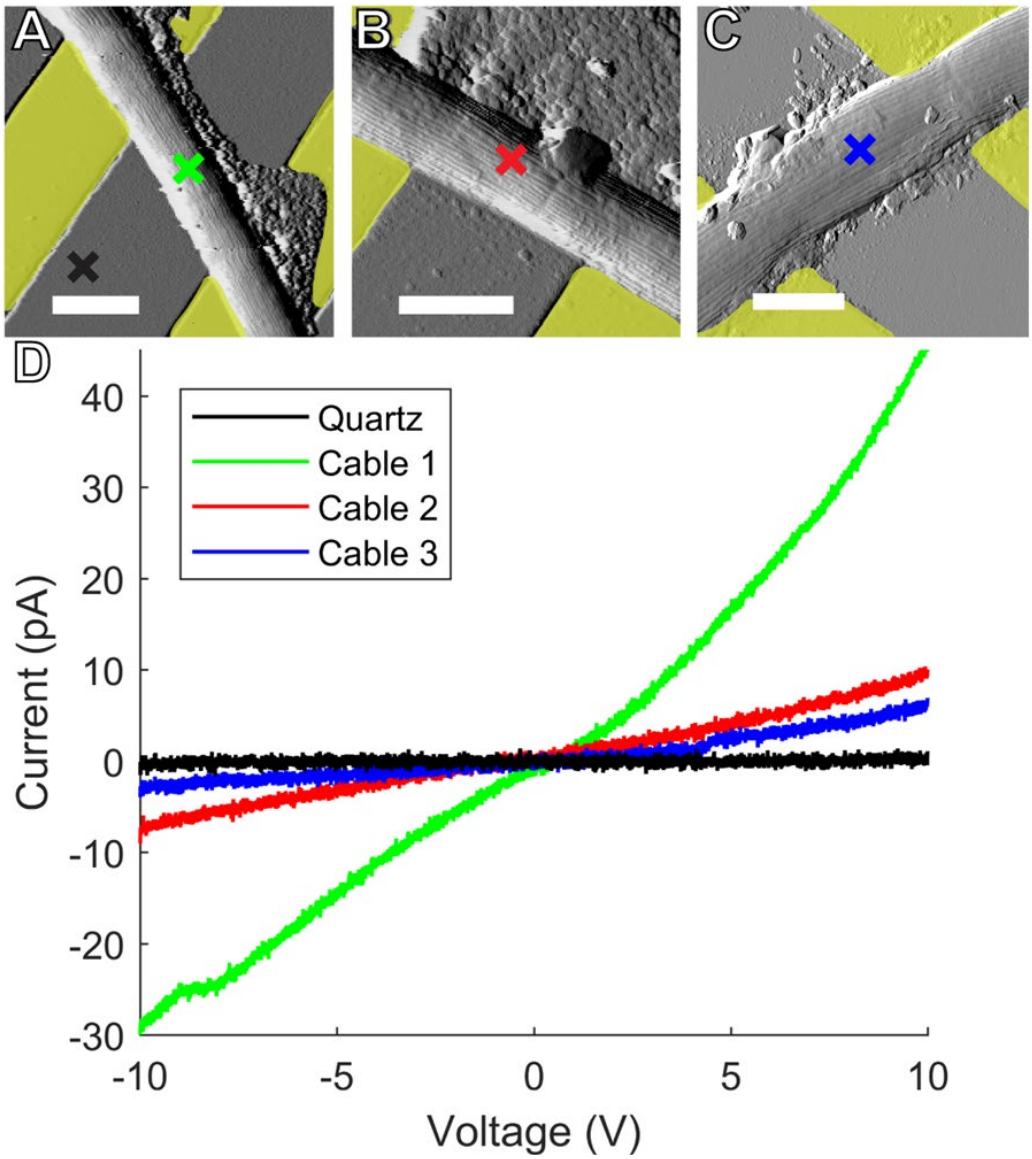

Figure 7. (A) A spatial montage of three consecutive tapping atomic force microscopy amplitude images of two parallel Mungi Lake freshwater cable bacteria in contact with, and extending away from, an electrode (false colored yellow). Scale bar: 3 µm. **(B)** Conductive atomic force current map images of the same sections shown in (A) with 5 V bias between the underlying electrode and conductive tip. The observed current signals largely correlate with the corresponding cell surface ridge pattern in (A).

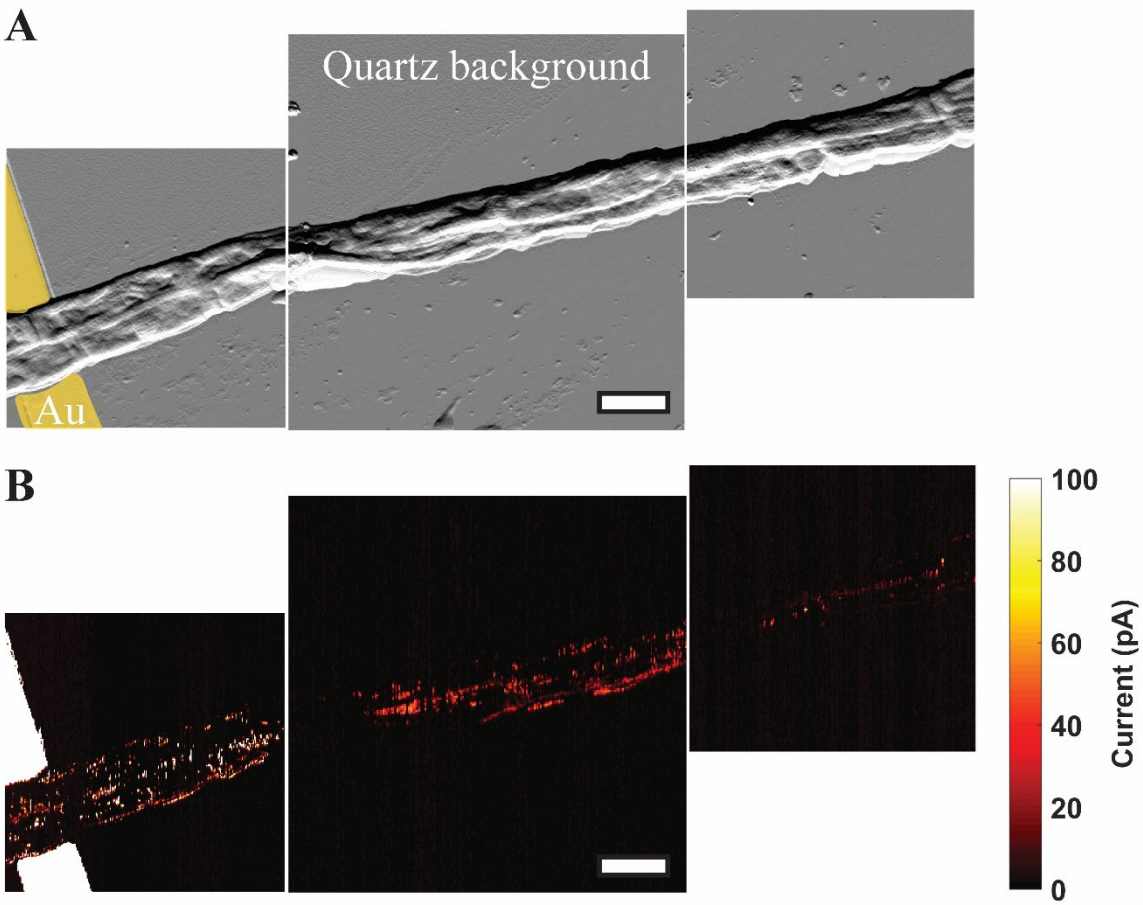

Figure 8. Four-probe current-voltage measurements of Mungi Lake freshwater cable bacteria filaments, shown for two different separations between the two inner probes. Inset: representative image of cable bacteria filaments across a four-probe device. Each data point is the average of three data points, and the error bars represent the standard deviation.

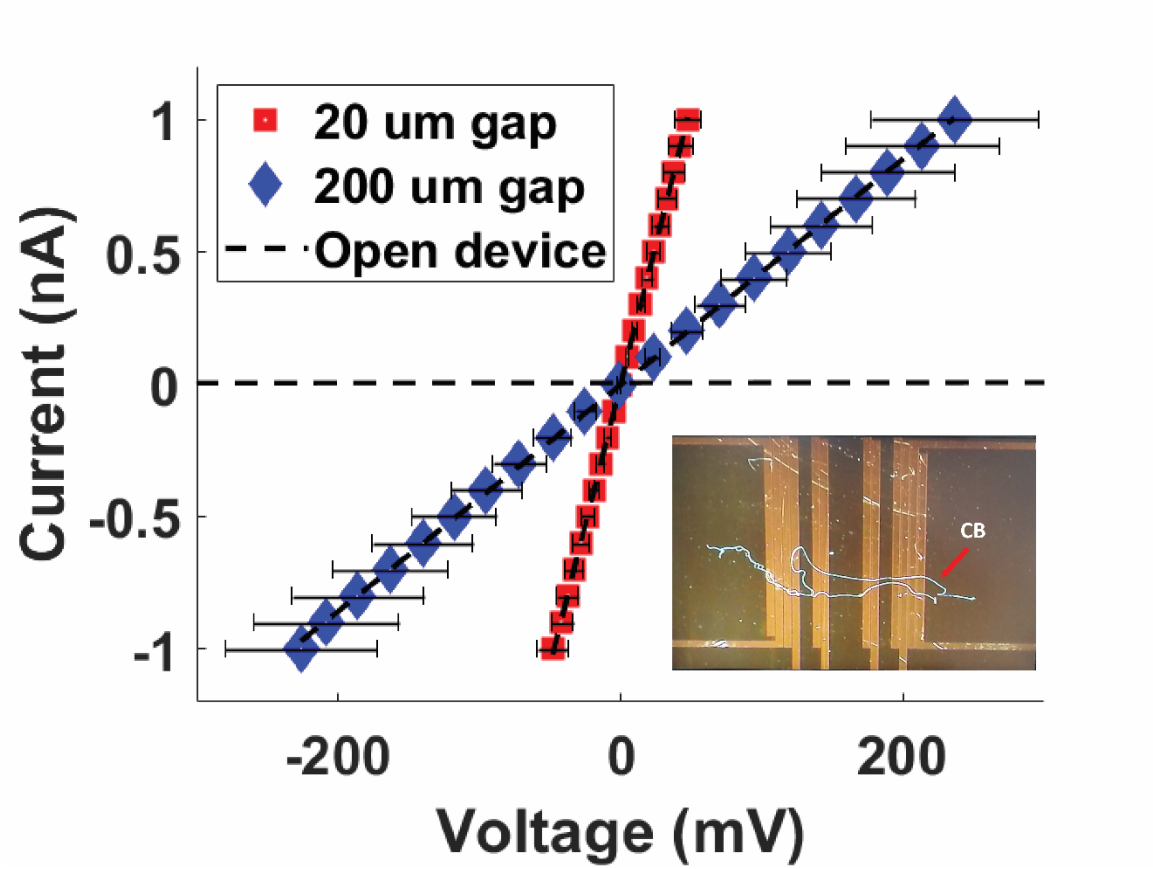
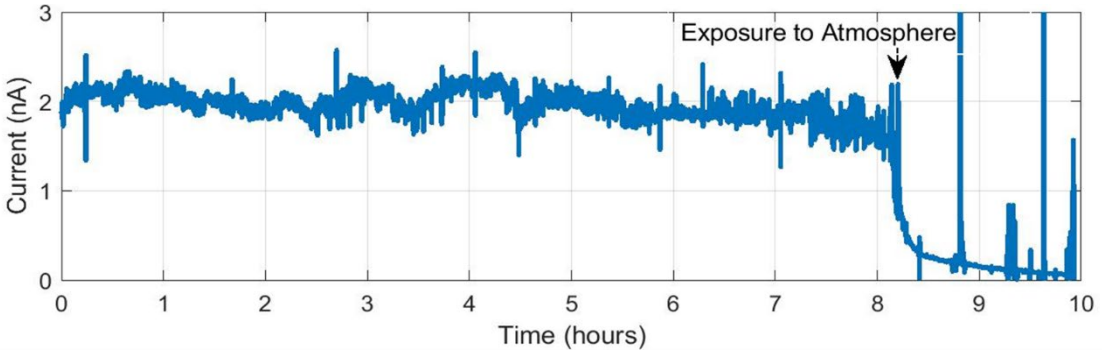
Figure S1. An example of sensitivity of conduction in cable bacteria to air exposure. Consistent current is monitored overnight for a Ballona freshwater sediment cable bacteria filament on an IDA under N_2 flow conditions, with an 800 mV difference between the two microelectrode bands. The current immediately declined upon interruption of N_2 flow and exposure to air.